THE JOURNAL OF PHYSICAL CHEMISTRY Letters

pubs.acs.org/JPCL Letter

Cryogenic "Iodide-Tagging" Photoelectron Spectroscopy: A Sensitive Probe for Specific Binding Sites of Amino Acids

Hanhui Zhang,[⊥] Wenjin Cao,[⊥] Qinqin Yuan, Xiaoguo Zhou, Marat Valiev, Steven R. Kass,* and Xue-Bin Wang*

Cite This: *J. Phys. Chem. Lett.* 2020, 11, 4346–4352 Read Online

ACCESS | Metrics & More | Article Recommendations | Supporting Information

ABSTRACT: This work showcases cryogenic and temperature-dependent "iodide-tagging" photoelectron spectroscopy to probe specific binding sites of amino acids using the glycine–iodide complex (Gly·I$^-$) as a case study. Multiple Gly·I$^-$ isomers were generated from ambient electrospray ionization and kinetically isolated in a cryogenic ion trap. These structures were characterized with temperature-dependent "iodide-tagging" negative ion photoelectron spectroscopy (NIPES), where iodide was used as the "messenger" to interpret electronic energetics and structural information of various Gly·I$^-$ isomers. Accompanied by theoretical computations and Franck–Condon simulations, a total of five cluster structures have been identified along with their various binding motifs. This work demonstrates that "iodide-tagging" NIPES is a powerful general means for probing specific binding interactions in biological molecules of interest.

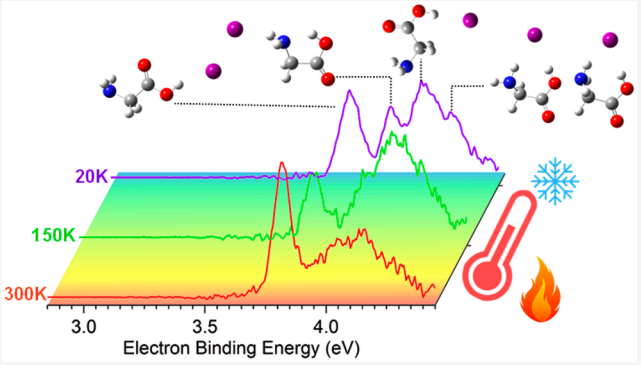

Downloaded via UNIV SCIENCE AND TECHNOLOGY CHINA on June 5, 2020 at 09:34:02 (UTC).
See https://pubs.acs.org/sharingguidelines for options on how to legitimately share published articles.

Amino acids (AAs) are well known fundamental components of proteins and have a variety of critical biological functions (e.g., as chemical messengers, energy metabolites, and essential nutrients). As a result, they are essential to human life and all other living things.[1,2] Their ion clusters along with protein–ion interactions are ubiquitous in nature and play a critical role in a variety of physiological processes.[3−8] For example, the essential process of ion concentration regulation occurs via ion transport through cell membranes and involves multiple protein–ion interactions. Both AA and protein–ion interactions are facilitated by the formation of zwitterionic structures in which the N-terminus or a basic side chain is protonated and the C-terminus is deprotonated.[9] In the absence of water, these isolated species are typically unstable in the gas phase,[10,11] but their zwitterionic forms can be stabilized by induction with numerous species such as a water molecule,[12−14] an electron,[15] or an ion.[16−24] This has led to an increase in the attention given to gas-phase spectroscopic studies of isolated AA–ion clusters, especially anionic ones with multiple binding sites due to the presence of several different hydrogen-bond donating groups.

Numerous conformers of AA-ion clusters exist and theoretical computations can be helpful in identifying those that are formed. Spectroscopic data, on the other hand, provide useful information to benchmark ab initio and density functional theory calculations.[25] Structural identification of AA-ion clusters via spectroscopy, nevertheless remains a challenging task. Two key issues are the extremely small population of thermodynamically less favorable structures and the difficulty in differentiating them. Conventional thermodynamic theories predict just the formation of the lowest energy isomer at low temperatures. That is, according to the well-accepted Boltzmann distribution law, species that are 1 kcal mol^{-1} higher in energy than the most stable structure contribute only ~10^{-3} % to the overall population at a temperature of 50 K. Moreover, most spectroscopic measurements are usually carried out at even lower temperatures. The other challenge is to distinguish different isomers with similar geometries and spectral profiles. This issue has been most commonly tackled by identifying signature vibrational modes of select isomers using techniques like infrared multiphoton dissociation (IRMPD).[19−23] Limitations in this methodology arise, however, with increasing molecular complexity as the number of possible structures increases and the vibrational spectra become more complicated.

In this Letter, we provide a new approach to probe-specific AA binding sites using a case study of the Gly·I$^-$ cluster anion

Received: April 8, 2020
Accepted: May 13, 2020
Published: May 13, 2020

© 2020 American Chemical Society

https://dx.doi.org/10.1021/acs.jpclett.0c01099
J. Phys. Chem. Lett. 2020, 11, 4346–4352

that addresses the two previously described challenges by generating these complexes using a top-down approach and characterizing them with "iodide-tagging" negative ion photoelectron spectroscopy (NIPES). In this top-down approach, Gly·I$^-$ anions are generated by electrospray ionization (ESI) under ambient conditions and guided into a cryogenic ion trap. Numerous accessible structures from room-temperature (RT) microsized droplets undergo rapid solvent evaporation cooling and collision cooling within the cryogenic ion trap and are kinetically isolated and retained. Cryogenic and temperature-dependent "iodide-tagging" NIPES is then used to characterize the resulting species. The name "iodide-tagging" is employed because of the important role I$^-$ plays as a messenger to interpret the NIPE spectra, which are expected to be dominated by atomic iodide transitions with two distinct bands separated by 0.94 eV arising from the $^2P_{3/2}$ and $^2P_{1/2}$ spin−orbit states of the iodine atom.[26,27] This characteristic spectral feature should make it possible to identify different isomers as resolved peaks with slightly different electron binding energies (EBEs) in the resulting complex spectrum. Confirmation of the presence of multiple species can be achieved by varying their relative populations by carrying out temperature-dependent measurements.[28−31] For the Gly·I$^-$ cluster, five distinct structures with different binding motifs and varying in energy over a 3.93 kcal mol^{-1} range were successfully trapped and characterized. The importance of iodide in cluster anions has recently been demonstrated and explored as a way to initiate intracluster electron transfer and study excited-state dynamics as well as to probe various tautomers of a specific biomolecule to which the iodide binds.[32−36]

In Figure 1, the 20 K NIPE spectra of the Gly·I$^-$ anion obtained with photon energies at both 266 (4.661 eV) and 193 nm (6.424 eV) are given. The latter spectrum exhibits two band systems originating at 3.71 and 4.66 eV (marked as Ω = 3/2 and 1/2 in Figure 1b) arising from the spin−orbit states (Ω = 3/2 and 1/2) of the neutral radical. The observed separation between these two bands is 0.95 eV, which is similar to the 0.942 eV splitting for atomic iodine[37] but with substantially higher EBEs than for I$^-$ (3.059 and 4.002 eV). This spectral pattern is similar to our previous observations with various iodide complexes,[26,27] suggesting that the electron is detached from a molecular orbital dominated by the I atom but is significantly stabilized by the binding of I$^-$ to glycine. A more complicated spectrum for the Gly·I$^-$ cluster results in that each of the two band systems exhibits multiple transitions over an EBE range of 0.8 eV. At least three features at 4.79, 5.00, and 5.13 eV with an unresolved shoulder at a higher EBE are observed in the Ω = 1/2 band system. In contrast, because of the higher electron kinetic energies in the lower EBE Ω = 3/2 band, this feature is less well-resolved but still exhibits a sharp band at 3.85 eV followed by a broad band with a maximum at 4.15 eV. The spectrum recorded at 266 nm affords significantly better resolution for the Ω = 3/2 band system due to the reduced electron kinetic energies. It clearly displays three well-resolved peaks at 3.85, 4.01, and 4.15 eV, respectively (marked as X, A, and B in Figure 1a) and a shoulder around 4.26 eV (marked as C in Figure 1a) at the higher EBE side of the 4.15 eV feature. Each of these four peaks has a corresponding signal within the Ω = 1/2 envelope with well-matching spacings for the expected spin−orbit splitting of the I atom (i.e., 0.94, 0.99, 0.98, and 0.96 eV, respectively). Because of this excellent one-to-one correspondence between the two band systems, only the features in the higher intensity and better resolved Ω = 3/2 envelope from the 266 nm spectrum were used in the following analyses.

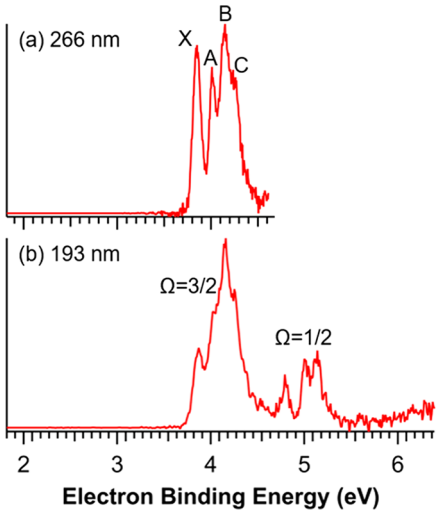

Figure 1. 20 K NIPE spectra of the Gly·I$^-$ anion obtained at (a) 266 and (b) 193 nm.

To assign the different features in the Ω = 3/2 band, one needs to consider vibrational coupling in a single species as well as different possible isomers. Given the unequal spacings between X, A, B, and C (i.e., 0.16, 0.14, and 0.11 eV, respectively) and their relative intensities, these features do not appear to be due to a vibrational progression. Additional insights were obtained with the aid of quantum-chemical calculations and the optimized B3LYP/aug-cc-pVDZ geometries of the low-lying structures of the Gly·I$^-$ anion, where the all-electron 6-311+G(df) basis set was used for the iodine, are given in Figure 2. Their calculated single-point relative energies and vertical detachment energies (VDEs) at the CCSD(T) level with the aug-cc-pVTZ (and aug-cc-pVTZ-PP for I) basis set are provided in Table 1. The six lowest energy isomers **1**−**6** adopt structures in which the glycine is in its canonical form, whereas its zwitterionic isomer **zw** has a higher relative energy of +7.49 kcal mol^{-1}.

Glycine has several different types of bonds to hydrogen (i.e., N−H, O−H, and C−H), and this leads to various hydrogen bond binding motifs to the iodide anion. Of the six lower-energy canonical structures, their relative energies exhibit a descending trend with an increase in the number of XH·I$^-$ interactions, where X = C, N, or O. The two most stable isomers, **1** and **2**, both have three hydrogen bonds to the iodide anion (i.e., two NH·I$^-$ and one OH·I$^-$ interaction for **1** and two CH·I$^-$ and one OH·I$^-$ hydrogen bond for **2**), and the latter species is 0.45 kcal mol^{-1} higher in energy. In comparison, both **3** and **4** have two hydrogen bonds (i.e., one NH·I$^-$ and one OH·I$^-$ interaction for **3** and two NH·I$^-$ hydrogen bonds for **4**), and they are 1.34 and 1.57 kcal mol^{-1} less stable. Isomers **5** and **6** both have one OH·I$^-$ interaction and have significantly higher energies of 3.93 and 5.10 kcal mol^{-1}. All of these structures, however, should be accessible at RT in the ESI solution used to generate the Gly·I$^-$ clusters.

The computed VDEs of **1**−**6** span from 3.83 to 4.30 eV and are all within the range of the observed Ω = 3/2 band system, whereas **zw** has a significantly higher calculated VDE of 4.86 eV (Table 1) and can be excluded from contributing to the

https://dx.doi.org/10.1021/acs.jpclett.0c01099
J. Phys. Chem. Lett. 2020, 11, 4346−4352

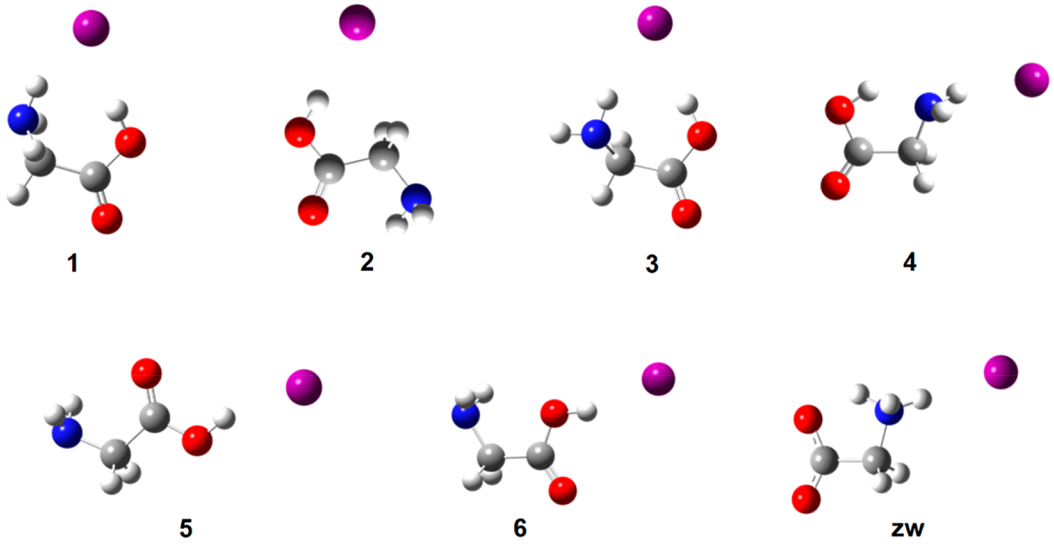

Figure 2. B3LYP optimized geometries of Gly·I⁻ complexes **1**−**6** and **zw** with the aug-cc-pVDZ basis set, except for iodine, which was treated with the 6-311+G(df) all-electron basis set.

Table 1. CCSD(T)//B3LYP Calculated Relative Energies (E, kcal mol^{-1}) and VDEs (eV) of Different Gly·I⁻ Structures along with Their Observed Experimental VDEs

	1	2	3	4	5	6	zw
E^a	0	0.45	1.34	1.57	3.93	5.10	7.49
VDE	4.30	4.16	4.30	3.96	3.83	3.86	4.86
expt.	4.26	4.15	4.26	4.01	3.85		

[a]ZPE corrections were carried out using the B3LYP vibrational frequencies.

266 nm photoelectron spectrum. The Franck−Condon factor (FCF) simulations based on each of these structures (Figure S1) further exclude the possibility that the multiple peaks in the band structure arise from vibrational coupling. That is, the FCF simulated spectra for **2**−**6** are all dominated by sharp transitions for the VDEs starting at their EBEs. Isomer **1** exhibits a broad band between 4.1 and 4.5 eV arising from the excitations of different vibrational modes of the neutral radical, including NH_2-related modes (NH_2 twisting, rocking, and wagging as well as N−H stretching), I-glycine stretching, and N−C−C/C−O−H bending of the glycine motif. However, it cannot reproduce the observed spectrum that is spread out over a ∼0.8 eV range. Zwitterion **zw** has a broad simulated spectrum that covers the requisite energy range, but given its relatively low stability and large calculated VDE of 4.86 eV, this isomer is also excluded as a candidate that can reproduce the experimental bands by itself. Each of the calculated VDEs of **1**−**6**, however, match one of the four observed features in the Ω = 3/2 band, and this strongly suggests that the spectrum arises from the presence of multiple isomers of the Gly·I⁻ cluster.

On the basis of the above analyses and the excellent agreement between the experimental and calculated VDE band positions, the four peaks in the Ω = 3/2 band system are assigned to vertical transitions of anions **1**−**5** to their neutral ground states. Both **1** and **3** are assigned to band C at 4.26 eV because they have identical calculated VDEs of 4.30 eV. The observed X, A, and B bands at 3.85, 4.01, and 4.15 eV are assigned to **5**, **4**, and **2**, respectively, given their computed VDEs of 3.83, 3.96, and 4.16 eV. Clusters **6** and **zw** are predicted to be less stable than the other species, and in the former case, its predicted VDE overlaps with **5**, whereas it falls in the Ω = 1/2 band for **zw**. Given the observed spectral resolution and for simplicity's sake, we decided to neglect these latter two isomers from the simulated 266 nm spectrum obtained by combining the FCF simulations of **1**−**5** (Figure 3). An excellent match was obtained by normalizing each

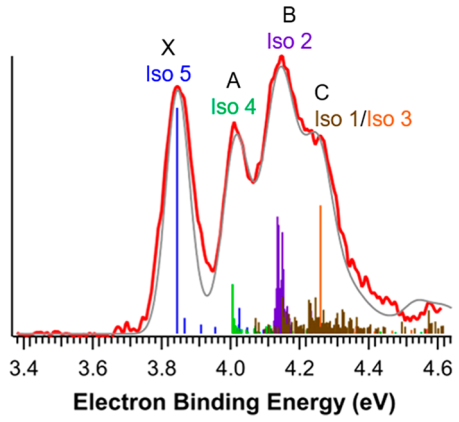

Figure 3. Simulated NIPE spectrum (gray) using the calculated stick spectra (brown, violet, orange, green, and blue for **1**−**5**, respectively) convoluted with Gaussian line broadening (where the fwhm's of each Gaussian were set to 60 meV) superimposed onto the experimental 266 nm spectrum (red). The simulated spectra for each individual structure compared with the experimental spectrum are provided in Figure S1.

contributor's contribution to the experimental peak height and only adjusting their weights due to peak overlap. The strong intensity of band X corresponds to **5** with a relative energy of 3.93 kcal mol^{-1}, and this might seem to violate the Boltzmann distribution law, but the height of a given band is determined by the population of a given isomer and its photodetachment cross section as well as the spectral overlap. Considering the weaker interaction between glycine and I⁻ in **5** and that there is only one hydrogen bond to the iodide, it is feasible that the photodetachment cross-section of this isomer is larger than those for **1**−**4**.

https://dx.doi.org/10.1021/acs.jpclett.0c01099
J. Phys. Chem. Lett. 2020, 11, 4346−4352

The relative intensities of different features in NIPE spectra do not directly reflect population distributions, but changes in the intensities as a function of temperature should provide a measure of the various chemical structures thermodynamic stabilities. Consequently, the 266 nm spectra of the Gly·I$^-$ anion were obtained at temperatures ranging from 20 to 300 K (Figure 4), and the relative intensities of the X, A, B, and C

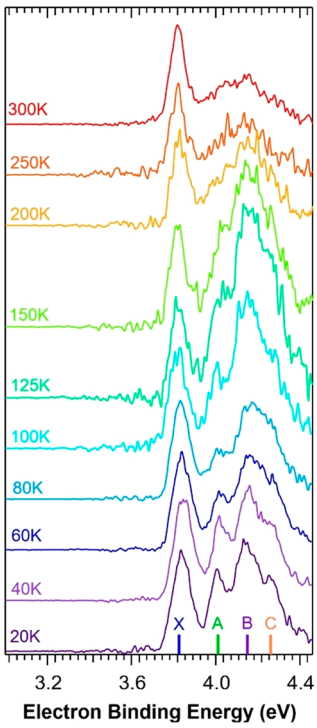

Figure 4. Temperature-dependent NIPE spectra of Gly·I$^-$ at 266 nm.

bands at each temperature after normalizing the total intensity of each spectrum are illustrated in Figure 5. The room-temperature spectrum (300 K) is dominated by X with a ratio of 0.46, but this feature gradually diminishes as the temperature is lowered and reaches a minimum value of 0.17 at 125 K. In contrast, bands A, B, and C increase in intensity

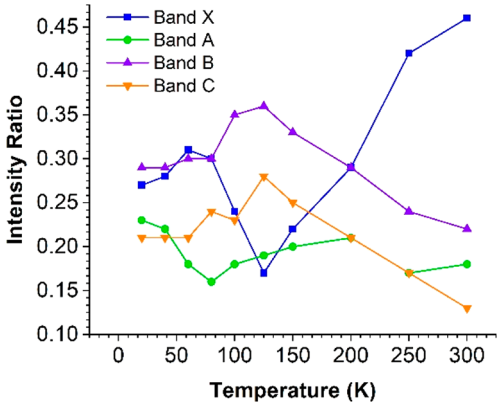

Figure 5. Intensity ratios of X, A, B, and C in the 266 nm NIPE spectra of Gly·I$^-$ as a function of temperature from 20−300 K. The total intensities for each of the spectra were normalized, and the given ratios were estimated based on peak heights. Given that the spectral resolution and intensity of band A decrease with increasing temperature, these results are only qualitative in nature.

over this temperature range (300−125 K). At lower temperatures, these trends break down and are reversed from 125 to 80 K (i.e., the intensity ratio of X increases, and those for A, B, and C decrease); then, a "plateau" region is reached below 80 K, where the intensity ratios remain almost unchanged, except for band A, which slightly increases. Our computations indicate that **5** is the energetically least stable conformer but has the largest and most favorable entropy (96.79 cal mol^{-1} K^{-1}, Table S1) due to its greater structural flexibility resulting from having only one hydrogen bond to the iodide ion. As a result, its relative Gibbs free energy of formation (Δ_fG) decreases with increasing temperature, resulting in a more favorable population at higher temperatures. At 300 K, Δ_fG for **5** is still 2.73 kcal mol^{-1} larger than that for **1**, and whereas its relative population is predicted to be smaller than those of **1**−**4**, it will be greatly enhanced based on the Boltzmann distribution law. As a result, it is not surprising to see an increase in the intensity ratio of X and decreases in the other bands in going from 125 to 300 K. The unexpected trends at even lower temperatures can be attributed to the rapid cooling of the cluster ions and the insufficient energy to readily overcome interconversion barriers leading to the equilibration of the different isomeric structures. As a result, these species are kinetically trapped and isolated, leading to populations that differ from those predicted on the basis of the Boltzmann distribution law. It is worth noting that by changing the different solvents used in ESI, the population of each isomer formed in the ion source can be varied to a certain extent.[38,39] However, temperature-dependent measurements hold the capabilities of not only changing the relative intensities of different isomers but also providing thermodynamic entropy information.

The Gly·I$^-$ complex represents one of the simplest cases in ion−biomolecule interactions, yet our study has demonstrated a richness and diversity in its binding motifs. This was achieved via the cryogenic and temperature-dependent photoelectron spectroscopic characterization of multiple kinetically trapped isomers using iodide as a "messenger" to interpret the energetic and structural properties of an anion−AA cluster. Taking advantage of the simplicity of the spectral profile of such complexes, multiple isomers can be identified based on their different VDEs and temperature-dependent intensity ratios. This enables the binding sites in these species to be determined and should facilitate the understanding of anion−protein interactions. Furthermore, this technique could be extremely useful in probing zwitterionic forms of AAs stabilized by interactions with other molecules or ions in the gas phase that have been computationally predicted but still experimentally unconfirmed.[40−42] We can envision synthesizing the iodide counterparts of these AA−anion complexes by substituting the "anion moiety" with iodide and performing cryogenic and temperature-dependent NIPES experiments on those AA·I$^-$ clusters. The resulting spectrum should encode spectroscopic signatures on different iodide binding sites of canonical or zwitterionic AAs. Although not directly identifying the iodide-induced zwitterionic glycine structure in this work, the power in determining multiple isomeric structures with a several kcal mol^{-1} energy window and a high detection sensitivity offers new possibilities for investigating zwitterion and canonical motifs and the effect of additional charge centers or solvent molecules.

In summary, we have reported a case study on the Gly·I$^-$ complex using cryogenic and temperature-dependent "iodide-

https://dx.doi.org/10.1021/acs.jpclett.0c01099
J. Phys. Chem. Lett. 2020, 11, 4346−4352

tagging" photoelectron spectroscopy combined with theoretical computations. A total of five isomers with computed CCSD(T) relative energies spanning 3.93 kcal mol^{-1} have been successfully trapped and characterized on the basis of the excellent agreement between experimental and calculated VDEs, well-matched FCF simulated spectra with the measured spectrum, and the agreement between theoretically computed thermodynamics properties and experimentally observed population variations with temperature. This investigation has revealed diverse binding motifs between glycine and iodide. Structures with three hydrogen bonds to I^- are energetically more stable than those with fewer hydrogen bonds, but they are more oriented and entropically less favorable, leading to a diminishment of their populations at higher temperatures.

EXPERIMENTAL METHODS

This work was performed with the Pacific Northwest National Laboratory (PNNL) ESI-NIPES apparatus utilizing a temperature-controlled cryogenic ion trap.[28] Gly·I^- anions were produced via electrospraying a ∼0.1 mM mixture of both KI and glycine in a 3:1 v/v ratio of acetonitrile/water. These cluster anions were generated at RT and then accumulated and cooled in a 3D Paul trap. The cold ions were then pulsed out into the extraction zone of a time-of-flight mass spectrometer at a repetition rate of 10 Hz. Mass-selected anions were decelerated and photodetached by a laser beam in the photodetachment zone of the magnetic bottle photoelectron analyzer. Either a 266 nm (4.661 eV) Nd:YAG laser or a 193 nm (6.424 eV) ArF excimer laser was used, operating at a 20 Hz repetition rate with the ion beam off on alternating laser shots to afford shot-by-shot background subtraction. The photodetached electrons were collected at nearly 100% efficiency by the magnetic bottle and analyzed in a 5.2 m long electron flight tube. Time-of-flight NIPE spectra were collected and then converted into electron kinetic energy spectra by calibration with the known spectra of $I^-/OsCl_6^{2-}$ or $I^-/Cu(CN)_2^-$. Electron binding energies were subsequently obtained by subtracting the electron kinetic energies from the detachment photon energies. These spectra have an electron energy resolution ($E/\Delta E$) of ∼2% (i.e., ∼20 meV for 1 eV kinetic energy electrons).

Theoretical Details. Numerous initial structures for the Gly·I^- cluster anions in zwitterionic and canonical forms were systematically examined with molecular dynamics searches using semiempirical methods (AM1[43] and PM3[44]) with the Spartan software.[45] All conformations within 10 kcal mol^{-1} of the most stable one were used as initial structures for subsequent optimizations. Further geometry optimizations and harmonic frequency analyses of all candidate anions and corresponding neutral radicals were performed with density functional theory (DFT) using the B3LYP functional[46,47] without any symmetry constraints, as this approach was previously found to be effective.[48,49] The 6-311+G(df) all-electron basis set was used for iodine, and the aug-cc-pVDZ basis set[50] was used for all other atoms. Vibrational frequency analyses ensured that the optimized structures are true energy minima on the potential energy surface. The energies of each optimized anion and corresponding neutral radical at the anion geometry were refined by CCSD(T)[51,52] single-point energy calculations with the aug-cc-pVTZ[50] (and aug-cc-pVTZ-PP[53] for I) basis set. VDEs were calculated as the energy differences between the neutral and anionic clusters, both at the optimized anion geometries, whereas the relative energies of different anion isomers were calculated based on their electronic energies with zero-point energy (ZPE) corrections at the DFT level. All DFT calculations were performed with the Gaussian 03 software[54] package, whereas the CCSD(T) calculations were done with MOLPRO 2015.1.[55] Additionally, the FCFs for spectral simulations including Duschinsky rotations were computed with the ezSpectrum program.[56]

ASSOCIATED CONTENT

Supporting Information

The Supporting Information is available free of charge at https://pubs.acs.org/doi/10.1021/acs.jpclett.0c01099.

Figure S1. Experimental NIPE spectra of Gly·I^- and simulated stick and convoluted spectra of six low-energy canonical structures and the most favorable zwitterionic form. Table S1. Computed entropies and Gibbs free energies of formation for **1**−**5** at temperatures ranging from 20 to 300 K (PDF)

AUTHOR INFORMATION

Corresponding Authors

Xue-Bin Wang − *Physical Sciences Division, Pacific Northwest National Laboratory, Richland, Washington 99352, United States;* orcid.org/0000-0001-8326-1780; Email: xuebin.wang@pnnl.gov

Steven R. Kass − *Department of Chemistry, University of Minnesota, Minneapolis, Minnesota 55455, United States;* orcid.org/0000-0001-7007-9322; Email: kass@umn.edu

Authors

Hanhui Zhang − *Physical Sciences Division, Pacific Northwest National Laboratory, Richland, Washington 99352, United States; Hefei National Laboratory for Physical Sciences at the Microscale, Department of Chemical Physics, University of Science and Technology of China, Hefei, Anhui 230026, P. R. China*

Wenjin Cao − *Physical Sciences Division, Pacific Northwest National Laboratory, Richland, Washington 99352, United States;* orcid.org/0000-0002-2852-4047

Qinqin Yuan − *Physical Sciences Division, Pacific Northwest National Laboratory, Richland, Washington 99352, United States*

Xiaoguo Zhou − *Hefei National Laboratory for Physical Sciences at the Microscale, Department of Chemical Physics, University of Science and Technology of China, Hefei, Anhui 230026, P. R. China;* orcid.org/0000-0002-0264-0146

Marat Valiev − *Environmental Molecular Sciences Laboratory, Pacific Northwest National Laboratory, Richland, Washington 99352, United States;* orcid.org/0000-0001-6127-1988

Complete contact information is available at: https://pubs.acs.org/10.1021/acs.jpclett.0c01099

Author Contributions

⊥H.Z. and W.C. contributed equally to this work.

Notes

The authors declare no competing financial interest.

ACKNOWLEDGMENTS

This work was supported by the U.S. Department of Energy (DOE), Office of Basic Energy Sciences, Division of Chemical Science, Geosciences, and Biosciences and was performed

using EMSL, a national scientific user facility sponsored by DOE's Office of Biological and Environmental Research and located at Pacific Northwest National Laboratory, which is operated by the Battelle Memorial Institute for the DOE. The theoretical calculations were conducted on the EMSL Cascade Supercomputer and at the University of Minnesota Supercomputing Institute. S.R.K. acknowledges support from the National Science Foundation (CHE-1361766). The financial support from the Ministry of Science and Technology of China (no. 2012YQ220113) is also gratefully acknowledged (X.Z.).

REFERENCES

(1) Loo, J. A. Studying Noncovalent Protein Complexes by Electrospray Ionization Mass Spectrometry. *Mass Spectrom. Rev.* **1997**, *16*, 1−23.
(2) Pyle, A. Metal Ions in the Structure and Function of RNA. *J. Biol. Inorg. Chem.* **2002**, *7*, 679−690.
(3) Chesler, M. Regulation and Modulation of pH in the Brain. *Physiol. Rev.* **2003**, *83*, 1183−1221.
(4) Dashper, S.; Brownfield, L.; Slakeski, N.; Zilm, P.; Rogers, A.; Reynolds, E. Sodium Ion-Driven Serine/Threonine Transport in Porphyromonas Gingivalis. *J. Bacteriol.* **2001**, *183*, 4142−4148.
(5) Frings, S.; Reuter, D.; Kleene, S. Neuronal Ca^{2+}-Activated Cl^- Channels—Homing in on an Elusive Channel Species. *Prog. Neurobiol.* **2000**, *60*, 247−289.
(6) Kleene, S. J.; Gesteland, R. C. Calcium-Activated Chloride Conductance in Frog Olfactory Cilia. *J. Neurosci.* **1991**, *11*, 3624−3629.
(7) Firestein, S.; Shepherd, G. M. Interaction of Anionic and Cationic Currents Leads to a Voltage Dependence in the Odor Response of Olfactory Receptor Neurons. *J. Neurophysiol.* **1995**, *73*, 562−567.
(8) Delay, R.; Dubin, A.; Dionne, V. A Cyclic Nucleotide-Dependent Chloride Conductance in Olfactory Receptor Neurons. *J. Membr. Biol.* **1997**, *159*, 53−60.
(9) Locke, M. J.; McIver, R. T., Jr Effect of Solvation on the Acid/Base Properties of Glycine. *J. Am. Chem. Soc.* **1983**, *105*, 4226−4232.
(10) Marchese, R.; Grandori, R.; Carloni, P.; Raugei, S. On the Zwitterionic Nature of Gas-Phase Peptides and Protein Ions. *PLoS Comput. Biol.* **2010**, *6*, No. e1000775.
(11) Barran, P. E.; Polfer, N. C.; Campopiano, D. J.; Clarke, D. J.; Langridge-Smith, P. R.; Langley, R. J.; Govan, J. R.; Maxwell, A.; Dorin, J. R.; Millar, R. P.; et al. Is it Biologically Relevant to Measure the Structures of Small Peptides in the Gas-Phase? *Int. J. Mass Spectrom.* **2005**, *240*, 273−284.
(12) Jensen, J. H.; Gordon, M. S. On the Number of Water Molecules Necessary to Stabilize the Glycine Zwitterion. *J. Am. Chem. Soc.* **1995**, *117*, 8159−8170.
(13) Xu, S.; Nilles, J. M.; Bowen, K. H., Jr Zwitterion Formation in Hydrated Amino Acid, Dipole Bound Anions: How Many Water Molecules are Required? *J. Chem. Phys.* **2003**, *119*, 10696−10701.
(14) Bush, M. F.; Prell, J. S.; Saykally, R. J.; Williams, E. R. One Water Molecule Stabilizes the Cationized Arginine Zwitterion. *J. Am. Chem. Soc.* **2007**, *129*, 13544−13553.
(15) Gutowski, M.; Skurski, P.; Simons, J. Dipole-Bound Anions of Glycine Based on the Zwitterion and Neutral Structures. *J. Am. Chem. Soc.* **2000**, *122*, 10159−10162.
(16) Bush, M. F.; O'Brien, J. T.; Prell, J. S.; Saykally, R. J.; Williams, E. R. Infrared Spectroscopy of Cationized Arginine in the Gas Phase: Direct Evidence for the Transition from Nonzwitterionic to Zwitterionic Structure. *J. Am. Chem. Soc.* **2007**, *129*, 1612−1622.
(17) Lemoff, A. S.; Bush, M. F.; Williams, E. R. Binding Energies of Water to Sodiated Valine and Structural Isomers in the Gas Phase: The Effect of Proton Affinity on Zwitterion Stability. *J. Am. Chem. Soc.* **2003**, *125*, 13576−13584.
(18) Wyttenbach, T.; Witt, M.; Bowers, M. T. On the Stability of Amino Acid Zwitterions in the Gas Phase: The Influence of Derivatization, Proton Affinity, and Alkali Ion Addition. *J. Am. Chem. Soc.* **2000**, *122*, 3458−3464.
(19) Armentrout, P.; Rodgers, M.; Oomens, J.; Steill, J. Infrared Multiphoton Dissociation Spectroscopy of Cationized Serine: Effects of Alkali-Metal Cation Size on Gas-Phase Conformation. *J. Phys. Chem. A* **2008**, *112*, 2248−2257.
(20) Bush, M. F.; Oomens, J.; Saykally, R. J.; Williams, E. R. Effects of Alkaline Earth Metal Ion Complexation on Amino Acid Zwitterion Stability: Results from Infrared Action Spectroscopy. *J. Am. Chem. Soc.* **2008**, *130*, 6463−6471.
(21) Corinti, D.; Gregori, B.; Guidoni, L.; Scuderi, D.; McMahon, T. B.; Chiavarino, B.; Fornarini, S.; Crestoni, M. E. Complexation of Halide Ions to Tyrosine: Role of Non-Covalent Interactions Evidenced by IRMPD Spectroscopy. *Phys. Chem. Chem. Phys.* **2018**, *20*, 4429−4441.
(22) Schmidt, J.; Kass, S. R. Zwitterion vs Neutral Structures of Amino Acids Stabilized by a Negatively Charged Site: Infrared Photodissociation and Computations of Proline−Chloride Anion. *J. Phys. Chem. A* **2013**, *117*, 4863−4869.
(23) O'Brien, J. T.; Prell, J. S.; Berden, G.; Oomens, J.; Williams, E. R. Effects of Anions on the Zwitterion Stability of Glu, His and Arg Investigated by IRMPD Spectroscopy and Theory. *Int. J. Mass Spectrom.* **2010**, *297*, 116−123.
(24) Milner, E. M.; Nix, M. G.; Dessent, C. E. Collision-Induced Dissociation of Halide Ion−Arginine Complexes: Evidence for Anion-Induced Zwitterion Formation in Gas-Phase Arginine. *J. Phys. Chem. A* **2012**, *116*, 801−809.
(25) Walker, M.; Harvey, A. J.; Sen, A.; Dessent, C. E. Performance of M06, M06-2X, and M06-HF Density Functionals for Conformationally Flexible Anionic Clusters: M06 Functionals Perform Better than B3LYP for a Model System with Dispersion and Ionic Hydrogen-Bonding Interactions. *J. Phys. Chem. A* **2013**, *117*, 12590−12600.
(26) Hou, G.-L.; Wang, X.-B. Spectroscopic Signature of Proton Location in Proton Bound $HSO_4^-{\cdot}H^+{\cdot}X^-$ (X= F, Cl, Br, and I) Clusters. *J. Phys. Chem. Lett.* **2019**, *10*, 6714−6719.
(27) Wang, L.; Yuan, Q.; Cao, W.; Han, J.; Zhou, X.; Liu, S.; Wang, X.-B. Probing Orientation-Specific Charge-Dipole Interactions between Hexafluoroisopropanol and Halides: A Joint Photoelectron Spectroscopy and Theoretical Study. *J. Phys. Chem. A* **2020**, *124*, 2036−2045.
(28) Yuan, Q.; Cao, W.; Wang, X.-B. Cryogenic and Temperature-Dependent Photoelectron Spectroscopy of Metal Complexes. *Int. Rev. Phys. Chem.* **2020**, *39*, 83−108.
(29) Wang, X.-B.; Yang, J.; Wang, L.-S. Observation of Entropic Effect on Conformation Changes of Complex Systems under Well-Controlled Temperature Conditions. *J. Phys. Chem. A* **2008**, *112*, 172−175.
(30) Deng, S. H. M.; Kong, X.-Y.; Wang, X.-B. Probing the Early Stages of Salt Nucleation—Experimental and Theoretical Investigations of Sodium/Potassium Thiocyanate Cluster Anions. *J. Chem. Phys.* **2015**, *142*, 024313.
(31) Zagorec-Marks, W.; Foreman, M. M.; Verlet, J. R. R.; Weber, J. M. Cryogenic Ion Spectroscopy of the Green Fluorescent Protein Chromophore in Vacuo. *J. Phys. Chem. Lett.* **2019**, *10*, 7817−7822.
(32) Matthews, E.; Cercola, R.; Mensa-Bonsu, G.; Neumark, D. M.; Dessent, C. E. H. Photoexcitation of Iodide Ion-Pyrimidine Clusters Above the Electron Detachment Threshold: Intracluster Electron Transfer Versus Nucleobase-Centred Excitations. *J. Chem. Phys.* **2018**, *148*, 084304.
(33) Kunin, A.; McGraw, V. S.; Lunny, K. G.; Neumark, D. M. Time-Resolved Dynamics in Iodide-Uracil-Water Clusters upon Excitation of the Nucleobase. *J. Chem. Phys.* **2019**, *151*, 154304.
(34) Rogers, J. P.; Anstöter, C. S.; Bull, J. N.; Curchod, B. F. E.; Verlet, J. R. R. Photoelectron Spectroscopy of the Hexafluorobenzene Cluster Anions: $(C_6F_6)_n^-$ (n = 1−5) and $I^-(C_6F_6)$. *J. Phys. Chem. A* **2019**, *123*, 1602−1612.

https://dx.doi.org/10.1021/acs.jpclett.0c01099
J. Phys. Chem. Lett. 2020, 11, 4346−4352

(35) Cercola, R.; Matthews, E.; Dessent, C. E. H. Near-Threshold Electron Transfer in Anion-Nucleobase Clusters: Does the Identity of the Anion Matter? *Mol. Phys.* **2019**, *117*, 3001−3010.
(36) Cercola, R.; Uleanya, K. O.; Dessent, C. E. H. Electron Detachment Dynamics of the Iodide-Guanine Cluster: Does Ionization Occur from the Iodide or from Guanine? *Mol. Phys.* **2019**, 1−10.
(37) Cheng, M.; Feng, Y.; Du, Y.; Zhu, Q.; Zheng, W.; Czakó, G.; Bowman, J. M. Communication: Probing the Entrance Channels of the X + CH_4 → HX + CH_3 (X= F, Cl, Br, I) Reactions via Photodetachment of X^-−CH_4. *J. Chem. Phys.* **2011**, *134*, 191102.
(38) Tian, Z.; Kass, S. R. Does Electrospray Ionization Produce Gas-Phase or Liquid-Phase Structures? *J. Am. Chem. Soc.* **2008**, *130*, 10842−10843.
(39) Matthews, E.; Dessent, C. E. H. Experiment and Theory Confirm that UV Laser Photodissociation Spectroscopy Can Distinguish Protomers Formed via Electrospray. *Phys. Chem. Chem. Phys.* **2017**, *19*, 17434−17440.
(40) Kass, S. R. Zwitterion−Dianion Complexes and Anion−Anion Clusters with Negative Dissociation Energies. *J. Am. Chem. Soc.* **2005**, *127*, 13098−13099.
(41) Yang, G.; Zu, Y.; Liu, C.; Fu, Y.; Zhou, L. Stabilization of Amino Acid Zwitterions with Varieties of Anionic Species: The Intrinsic Mechanism. *J. Phys. Chem. B* **2008**, *112*, 7104−7110.
(42) Tian, S. X.; Li, H. B.; Yang, J. Monoanion BH_4^- can Stabilize Zwitterionic Glycine with Dihydrogen Bonds. *ChemPhysChem* **2009**, *10*, 1435−1437.
(43) Dewar, M. J.; Zoebisch, E. G.; Healy, E. F.; Stewart, J. J. Development and Use of Quantum Mechanical Molecular Models. 76. AM1: A New General Purpose Quantum Mechanical Molecular Model. *J. Am. Chem. Soc.* **1985**, *107*, 3902−3909.
(44) Stewart, J. J. Optimization of Parameters for Semiempirical Methods II. Applications. *J. Comput. Chem.* **1989**, *10*, 221−264.
(45) *Spartan '08 for Macintosh*; Wavefunction, Inc.: Irvine, CA, 2008.
(46) Becke, A. D. Density-Functional Thermochemistry. III. The Role of Exact Exchange. *J. Chem. Phys.* **1993**, *98*, 5648−5652.
(47) Lee, C.; Yang, W.; Parr, R. G. Development of the Colle-Salvetti Correlation-Energy Formula into a Functional of the Electron Density. *Phys. Rev. B: Condens. Matter Mater. Phys.* **1988**, *37*, 785−789.
(48) Schmidt, J.; Kass, S. R. Zwitterion vs Neutral Structures of Amino Acids Stabilized by a Negatively Charged Site: Infrared Photodissociation and Computations of Proline-Chloride Anion. *J. Phys. Chem. A* **2013**, *117*, 4863−4869.
(49) Wang, X.-B.; Dacres, J. E.; Yang, X.; Lis, L.; Bedell, V. M.; Wang, L.-S.; Kass, S. R. Photodetachment of Zwitterions: Probing Intramolecular Coulomb Repulsion and Attraction in the Gas Phase Using Mono Decarboxylated Pyridinium Dicarboxylates. Implications on the Mechanism of Orotidine 5′-Monophosphate Decarboxylase. *J. Am. Chem. Soc.* **2003**, *125*, 6814−6826.
(50) Dunning, T. H., Jr Gaussian Basis Sets for Use in Correlated Molecular Calculations. I. The Atoms Boron Through Neon and Hydrogen. *J. Chem. Phys.* **1989**, *90*, 1007−1023.
(51) Purvis, G. D., III; Bartlett, R. J. A Full Coupled-Cluster Singles and Doubles Model: The Inclusion of Disconnected Triples. *J. Chem. Phys.* **1982**, *76*, 1910−1918.
(52) Raghavachari, K.; Trucks, G. W.; Pople, J. A.; Head-Gordon, M. A Fifth-Order Perturbation Comparison of Electron Correlation Theories. *Chem. Phys. Lett.* **1989**, *157*, 479−483.
(53) Peterson, K. A.; Shepler, B. C.; Figgen, D.; Stoll, H. On the Spectroscopic and Thermochemical Properties of ClO, BrO, IO, and Their Anions. *J. Phys. Chem. A* **2006**, *110*, 13877−13883.
(54) Frisch, M. J.; Trucks, G. W.; Schlegel, H. B.; Scuseria, G. E.; Robb, M. A.; Cheeseman, J. R.; Montgomery, J. A., Jr.; Vreven, T.; Kudin, K. N.; Burant, J. C.; et al. *Gaussian 03*, revision C.02; Gaussian, Inc.: Wallingford, CT, 2004.
(55) Werner, H.-J.; Knowles, P. J.; Knizia, G.; Manby, F. R.; Schütz, M.; Celani, P.; Györffy, W.; Kats, D.; Korona, T.; Lindh, R.; et al. *MOLPRO, Version 2015.1, A Package of Ab initio Programs*. http://www.molpro.net (accessed May 6, 2020).
(56) Mozhayskiy, V. A.; Krylov, A. I. *ezSpectrum*. http://iopenshell.usc.edu/downloads (accessed December 10, 2015).

https://dx.doi.org/10.1021/acs.jpclett.0c01099
J. Phys. Chem. Lett. 2020, 11, 4346−4352